Supporting information for

Structural Basis for Assembly and Activation of the Mn^{IV}/Fe^{III} Cofactor in the Class Ic Ribonucleotide Reductase from *Chlamydia trachomatis*

Table S1. Data collection and refinement statistics for apo β_2.

	apo β_2	apo β_2 (Fe ano)	apo β_2 (Mn ano)
Data collection			
Wavelength	1.078 Å	1.72 Å	1.86 Å
Space group	$P2_1$	$P2_1$	$P2_1$
Cell dimensions			
a, *b*, *c* (Å)	74.975, 97.394, 99.237	74.898, 97.431, 99.292	75.127, 97.711, 99.491
β (°)	97.760	97.683	97.691
Resolution (Å)	30.00-1.70 (1.73-1.70)	50.00-2.25 (2.29-2.25)	50.00-2.43 (2.47-2.43)
R_{sym} or R_{merge}	0.063 (0.749)	0.103 (0.359)	0.116 (0.447)
$I / \sigma I$	28.6 (1.9)	22.1 (6.4)	20.8 (5.0)
Completeness (%)	99.7 (97.7)	98.3 (96.2)	98.3 (96.2)
Redundancy	5.6 (4.1)	7.5 (7.2)	7.4 (6.2)
Refinement			
Resolution (Å)	30.00-1.70		
No. reflections	147567		
R_{work} / R_{free}	0.1794/0.2103		
No. atoms			
Protein	10946		
Ion/ligand	N/A		
Water	888		
B-factors			
Protein	21.0		
Ion/ligand	N/A		
Water	32.8		
r.m.s. deviations			
Bond lengths (Å)	0.008		
Bond angles (°)	1.015		

Table S2. Data collection and refinement statistics for Mn^{II}/Fe^{II}-β_2.

	Mn^{II}/Fe^{II}-β_2	Mn^{II}/Fe^{II}-β_2 (Fe ano)	Mn^{II}/Fe^{II}-β_2 (Mn ano)
Data collection			
Wavelength	1.078 Å	1.72 Å	1.86 Å
Space group	$P2_1$	$P2_1$	$P2_1$
Cell dimensions			
a, *b*, *c* (Å)	74.897, 97.455, 99.315	74.994, 97.813, 99.624	74.910, 97.373, 99.248
β (°)	97.765	97.777	97.746
Resolution (Å)	50.00-1.80 (1.83-1.80)	50.00-2.25 (2.29-2.25)	50.00-2.43 (2.47-2.43)
R_{sym} or R_{merge}	0.116 (0.497)	0.123 (0.499)	0.109 (0.338)
$I / \sigma I$	16.8 (2.9)	18.5 (3.8)	21.6 (5.8)
Completeness (%)	99.9 (98.9)	99.9 (99.2)	100.0 (99.6)
Redundancy	5.5 (4.0)	7.2 (5.1)	7.3 (6.1)
Refinement			
Resolution (Å)	50.00-1.80		
No. reflections	123898		
R_{work} / R_{free}	0.1725/0.2022		
No. atoms			
Protein	10889		
Metal	8		
Other ion/ligand	23		
Water	1027		
B-factors			
Protein	15.6		
Metal	16.7		
Other ion/ligand	39.6		
Water	28.5		
r.m.s. deviations			
Bond lengths (Å)	0.008		
Bond angles (°)	1.011		

Table S3. Data collection statistics for Mn^{II}-β_2 (1 equiv Mn^{II} per β).[a]

	Mn^{II}-β_2 (1 equiv)	Mn^{II}-β_2 (1 equiv) [Mn ano]
Data collection		
Wavelength	0.979 Å	1.860 Å
Space group	$P2_1$	$P2_1$
Cell dimensions		
a, *b*, *c* (Å)	74.905, 97.920, 100.391	75.371, 98.144, 100.704
β (°)	97.609	97.638
Resolution (Å)	50.00-1.76 (1.79-1.76)	50.00-2.42 (2.45-2.42)
R_{sym} or R_{merge}	0.077 (0.573)	0.085 (0.332)
$I / \sigma I$	24.7 (2.6)	29.2 (8.0)
Completeness (%)	99.0 (97.7)	97.2 (94.5)
Redundancy	7.6 (6.5)	7.7 (7.6)

[a]Crystallized aerobically by hanging drop vapor diffusion with 0.1 M HEPES, pH 7.2, 5% (w/v) PEG 3000, 0.2 M sodium acetate as the precipitant. Crystals were overlaid with cryoprotectant solution (well solution supplemented with 50% (v/v) glycerol) prior to data collection.

Table S4. Data collection statistics for Mn^{II}-β_2 (2 equiv Mn^{II} per β + 10 mM $MnCl_2$ soak).[a]

	Mn^{II}-β_2 (excess Mn^{II})	Mn^{II}-β_2 (excess Mn^{II}) [Mn ano]
Data collection		
Wavelength	0.979 Å	1.860 Å
Space group	$P2_1$	$P2_1$
Cell dimensions		
a, *b*, *c* (Å)	75.268, 98.029, 100.576	75.229, 97.967, 100.483
β (°)	97.765	97.742
Resolution (Å)	30.00-1.70 (1.73-1.70)	50.00-2.43 (2.47-2.43)
R_{sym} or R_{merge}	0.062 (0.691)	0.104 (0.404)
$I / \sigma I$	22.4 (2.1)	20.7 (6.4)
Completeness (%)	98.9 (97.7)	97.8 (95.2)
Redundancy	5.8 (5.6)	7.0 (7.5)

[a]Crystallized aerobically by hanging drop vapor diffusion with 0.1 M HEPES, pH 7.5, 20% (w/v) PEG 3000, 0.2 M sodium acetate as the precipitant. Crystals were overlaid with cryoprotectant solution (well solution supplemented with 50% (v/v) glycerol) prior to data collection.

Table S5. Data collection statistics for Mn^{IV}/Fe^{III}-β_2 (1 equiv Mn^{II} + 1 equiv Fe^{II} per β followed by exposure to excess O_2).

	Mn^{IV}/Fe^{III}-β_2 (1:1 Mn^{II}:Fe^{II})	Mn^{IV}/Fe^{III}-β_2 (1:1 Mn^{II}:Fe^{II}) [Fe ano]	Mn^{IV}/Fe^{III}-β_2 (1:1 Mn^{II}:Fe^{II}) [Mn ano]
Data collection			
Wavelength	1.033 Å	1.720 Å	1.860 Å
Space group	$P2_1$	$P2_1$	$P2_1$
Cell dimensions			
a, *b*, *c* (Å)	75.060, 96.630, 99.341	75.205, 96.752, 99.619	75.518, 96.987, 99.985
β (°)	98.236	98.217	98.571
Resolution (Å)	50.00-2.24 (2.28-2.24)	50.00-2.80 (2.85-2.80)	50.00-3.20 (3.26-3.20)
R_{svm} or R_{merge}	0.127 (0.690)	0.145 (0.735)	0.162 (0.723)
$I / \sigma I$	15.0 (2.2)	17.2 (2.0)	14.9 (2.6)
Completeness (%)	99.9 (97.7)	99.8 (96.6)	100.0 (99.9)
Redundancy	5.3 (3.5)	7.0 (4.3)	7.2 (5.2)

Table S6. Data collection statistics for Mn^{IV}/Fe^{III}-β_2 (2 equiv Mn^{II} + 0.65 equiv Fe^{II} per β followed by exposure to excess O_2).

	Mn^{IV}/Fe^{III}-β_2 (2:0.65 Mn^{II}:Fe^{II})	Mn^{IV}/Fe^{III}-β_2 (2:0.65 Mn^{II}:Fe^{II}) [Fe ano]	Mn^{IV}/Fe^{III}-β_2 (2:0.65 Mn^{II}:Fe^{II}) [Mn ano]
Data collection			
Wavelength	0.979 Å	1.720 Å	1.860 Å
Space group	$P2_1$	$P2_1$	$P2_1$
Cell dimensions			
a, *b*, *c* (Å)	75.277, 98.155, 100.707	75.277, 98.103, 100.637	75.219, 98.018, 100.624
β (°)	97.675	97.724	97.672
Resolution (Å)	30.00-1.90 (1.93-1.90)	50.00-2.11 (2.15-2.11)	50.00-2.15 (2.19-2.15)
R_{svm} or R_{merge}	0.060 (0.577)	0.111 (0.371)	0.065 (0.449)
$I / \sigma I$	18.9 (1.9)	21.3 (5.8)	29.1 (4.0)
Completeness (%)	99.3 (98.4)	100.0 (100.0)	100.0 (99.9)
Redundancy	3.2 (3.2)	7.3 (7.0)	7.4 (7.0)

Table S7. Data collection statistics for Mn^{II}/Fe^{II}-β_2 exposed to O_2 (ox. Mn^{II}/Fe^{II}-β_2).[a]

	ox. Mn^{II}/Fe^{II}-β_2
Data collection	
Wavelength	0.979 Å
Space group	$P2_1$
Cell dimensions	
a, *b*, *c* (Å)	75.130, 97.639, 100.039
β (°)	97.683
Resolution (Å)	50.00-1.68 (1.71-1.68)
R_{svm} or R_{merge}	0.085 (0.596)
$I / \sigma I$	19.6 (2.0)
Completeness (%)	99.8 (99.0)
Redundancy	5.6 (5.1)

[a]Crystallized by hanging drop vapor diffusion in an anaerobic chamber with 0.1 M HEPES, pH 7.0, 12% (w/v) PEG 3000, 0.2 M sodium acetate as the precipitant. The protein was adventitiously exposed to O_2 during crystallization or harvest. To prepare crystals for data collection, drops were overlaid with cryoprotectant solution (well solution supplemented with 40% (v/v) glycerol), and the resulting cryoprotectant-soaked crystals were mounted on rayon loops and frozen by immersion in liquid nitrogen.

Table S8. Data collection statistics for $Fe_2^{II/II}$-β_2 exposed to O_2 (ox. $Fe_2^{II/II}$-β_2).[a]

	ox. $Fe_2^{II/II}$-β_2
Data collection	
Wavelength	0.979 Å
Space group	$P2_1$
Cell dimensions	
a, *b*, *c* (Å)	75.296, 98.040, 100.373
β (°)	97.695
Resolution (Å)	50.00-2.00 (2.03-2.00)
R_{svm} or R_{merge}	0.084 (0.330)
$I / \sigma I$	20.1 (4.7)
Completeness (%)	95.7 (100.0)
Redundancy	5.6 (5.7)

[a]Crystallized by hanging drop vapor diffusion in an anaerobic chamber with 0.1 M HEPES, pH 7.2, 10% (w/v) PEG 3000, 0.2 M sodium acetate as the precipitant. The protein was adventitiously exposed to O_2 during crystallization or harvest. To prepare crystals for data collection, drops were overlaid with cryoprotectant solution (well solution supplemented with 40% (v/v) glycerol), and the resulting cryoprotectant-soaked crystals were mounted on rayon loops and frozen by immersion in liquid nitrogen.

Table S9. Anomalous peak heights (σ) at the Fe absorption edge for *Ct* β_2 crystallographic datasets. Note that these values are generated by a subtraction procedure to eliminate the contribution from Mn. The procedure fails to account for the decrease in Mn absorption with decreasing wavelength away from the Mn *K*-edge and results in a slight underestimate of the amount of Fe present at each site.

Crystal	Chain	Site 1	Site 2
Mn^{II}/Fe^{II}-β_2	A	2.9	14.3
	B	3.8	14.9
	C	2.2	12.7
	D	3.4	15.5
Mn^{IV}/Fe^{III}-β_2	A	2.9	10.6
procedure-3A	B	--	8.2
	C	--	5.4
	D	--	6.4
Mn^{IV}/Fe^{III}-β_2	A	--	6.2
procedure-3B	B	2.9	8.7
	C	--	6.0
	D	--	4.0

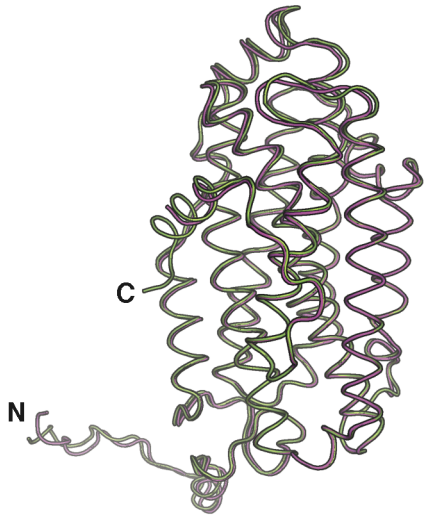

Figure S1. Secondary structure matching (SSM) superposition[1] for a representative β monomer from the apo *Ct* β_2 (pink), *Ct* Mn^{II}/Fe^{II}-β_2 (green) and *Ct* $Fe_2^{III/III}$-β_2 (PDB accession code 1SYY, not shown) crystal structures indicates a virtually identical overall fold among all three structures (0.46 Å rmsd for 317 Cα atoms).

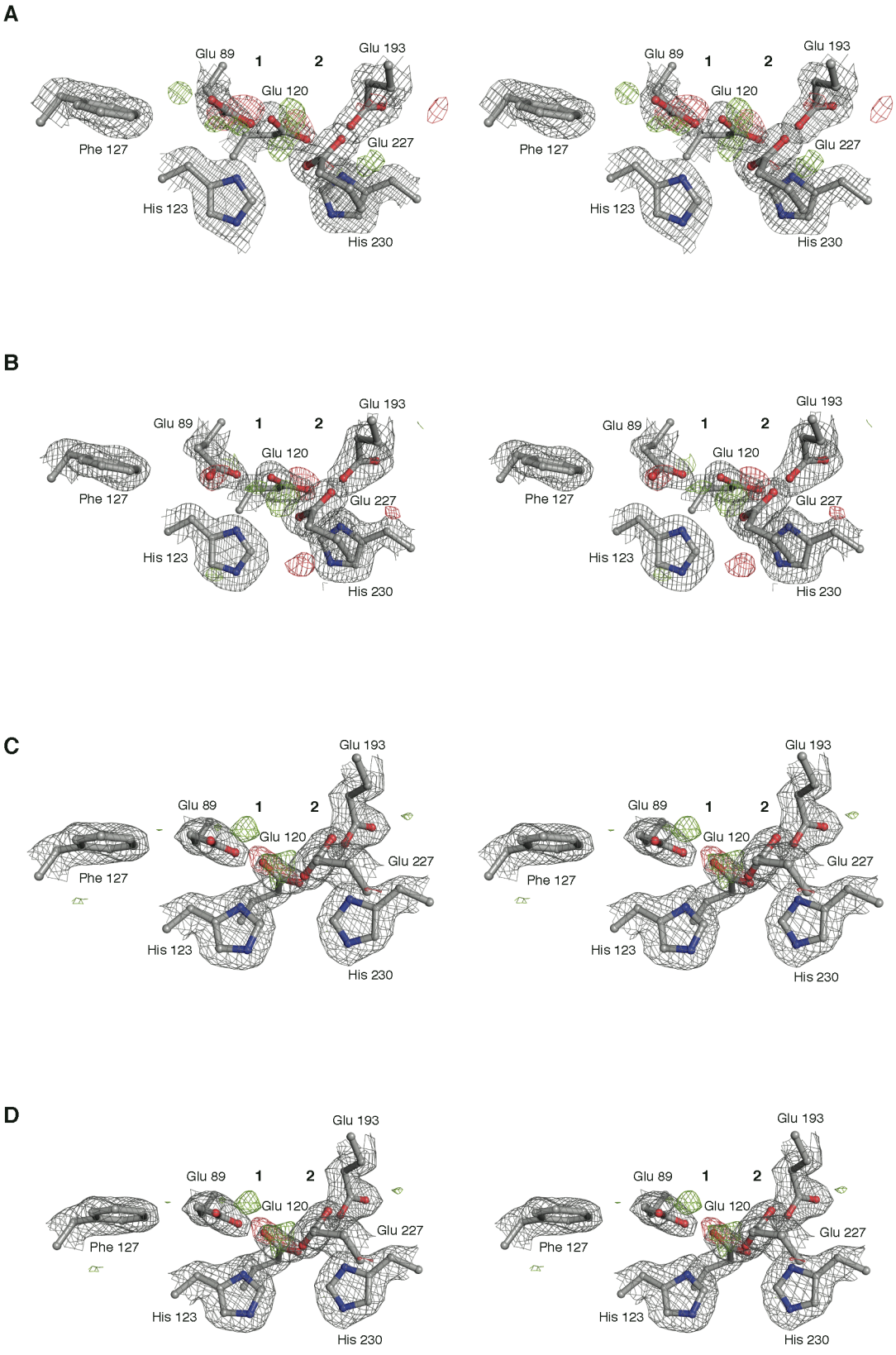
A
Glu 89
1
2
Glu 193
Glu 120
Phe 127
Glu 227
His 123
His 230
B
C
D

Figure S2. Stereo-views of the electron density map for the *Ct* apo β_2 metal binding site in each of the four β monomers in the ASU, designated chains A (**A**), B (**B**), C (**C**), and D (**D**). Selected protein side chains are shown in stick format. A $2F_o$-F_c map is shown in gray mesh (contoured at 1.2σ) and an F_o-F_c difference map is shown in red and green mesh (contoured at 3.0σ). Note minor amounts of difference density associated with Glu 89 and Glu 120, which may indicate partial disorder in the position of the side chains or the presence of disordered solvent nearby. Ordered waters were not modeled in the metal binding site due to the absence of $2F_o$-F_c density at a sufficient level in the initial electron density maps. Anomalous difference maps (data not shown) were also calculated from data collected at the Mn and Fe X-ray absorption edges (**Table S1**), and these are consistent with the absence of metal ions in the crystals, indicating that adventitious Mn or Fe does not account for any of this difference density.

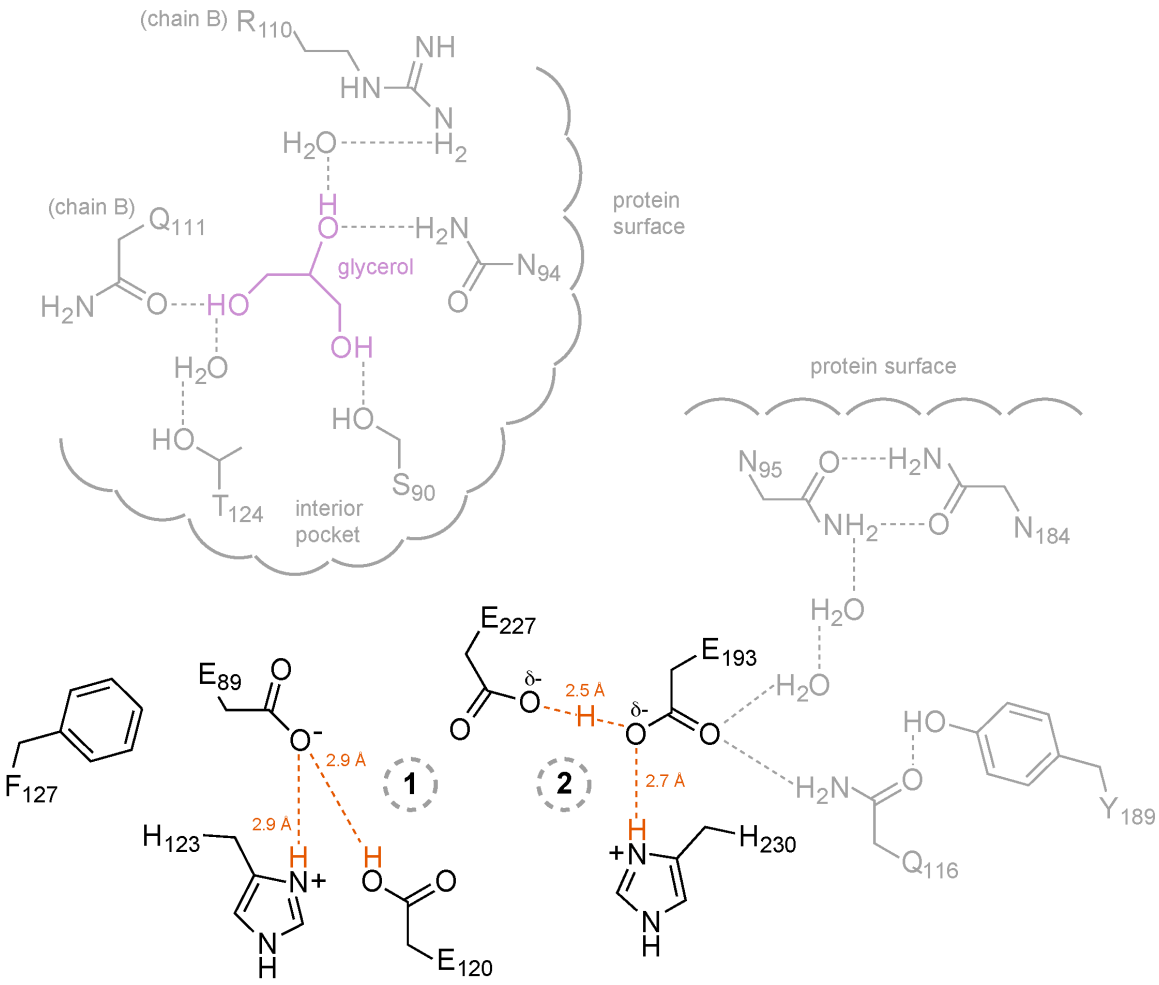

Figure S3. Schematic depiction of the cofactor site in apo β_2 and the surrounding residues which constitute two potential routes for proton efflux, metal influx, or both. Ligands and other selected residues are shown in black. Potential metal influx pathway residues are shaded in gray. Proposed protonation sites and potential hydrogen bonds among coordinating side chains are highlighted in red. A glycerol molecule observed in some crystallographic datasets (**Figure S9**) is shown in purple.

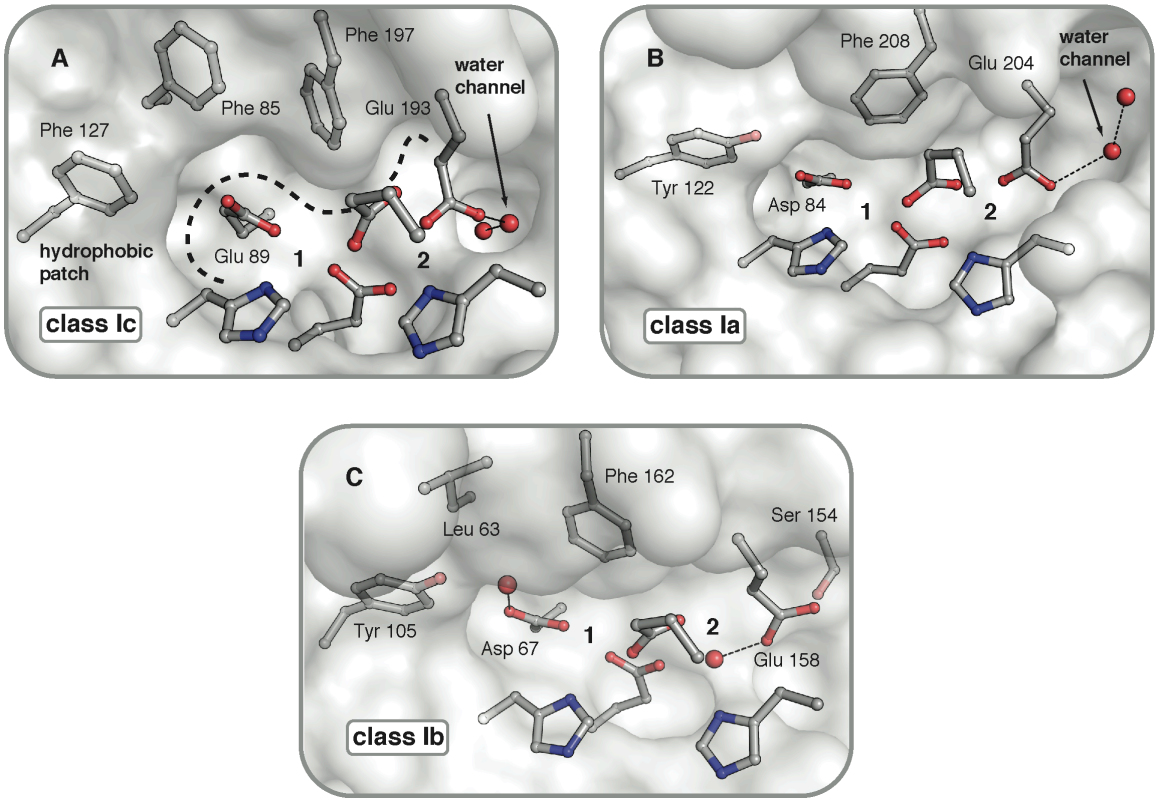

Figure S4. Second-sphere interactions of metal-binding ligands in class Ic apo β_2 (**A**) compared with apo class Ia (**B**)[2] and class Ib (PDB accession code 4M1F) (**C**) β_2 structures. Ligand residues are shown as sticks, and selected residues and water molecules outside the metal-binding site are shown in stick or sphere format, respectively. A cutaway view of the surrounding protein environment is shown as a transparent surface. This analysis reveals close steric packing around the ligands in class Ic β_2, defined primarily by a hydrophobic patch that surrounds site 1 and a short water channel that interacts with site 2, which brings the ligand residues closer together than in class Ia and Ib apo β_2 proteins. This feature of the surrounding protein environment may contribute to the absence of major conformational changes upon metal binding.

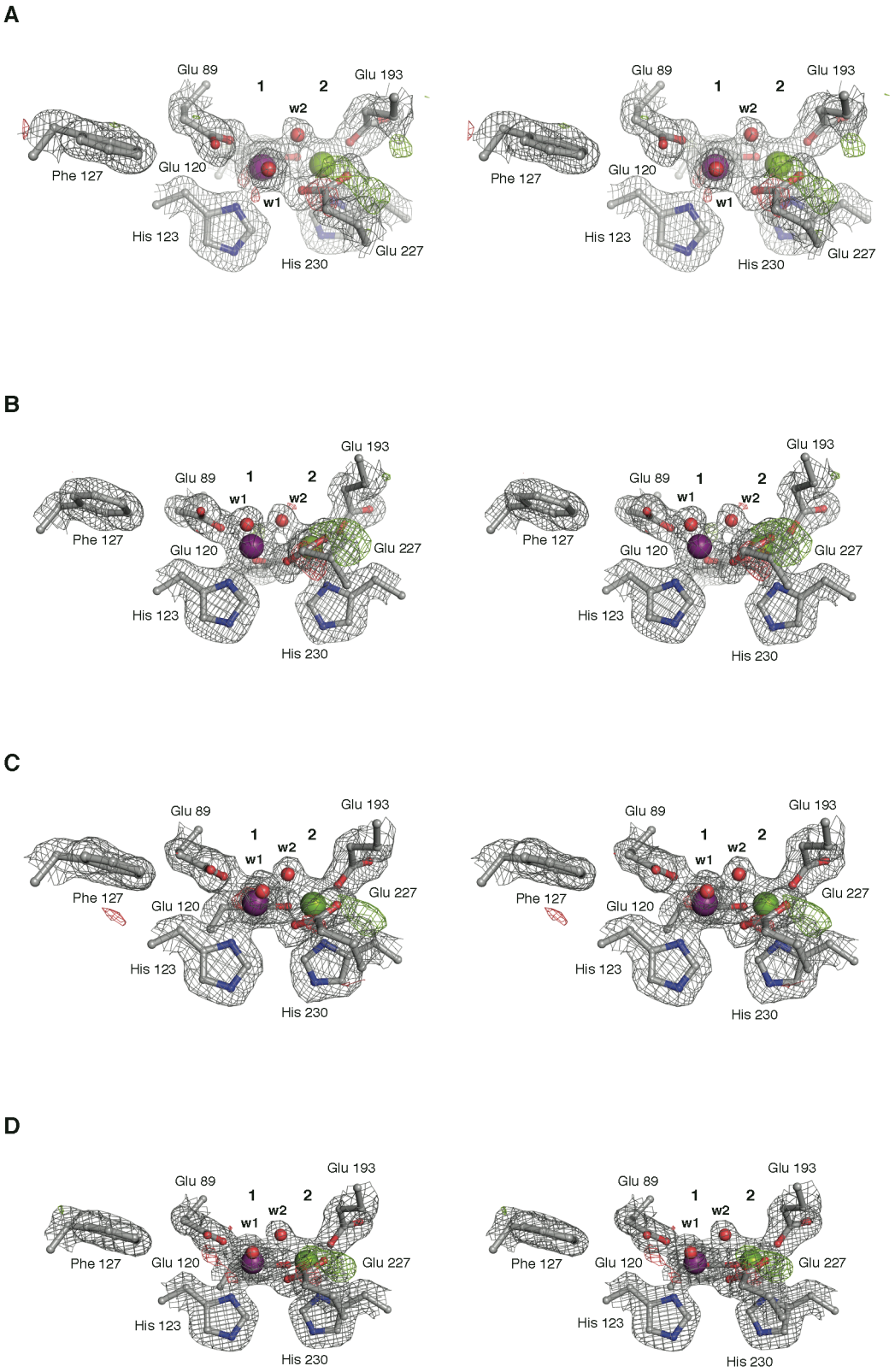

Figure S5. Stereoviews of the electron density map for the Mn^{II}/Fe^{II}-β_2 metal-binding site in each of the four β monomers in the ASU designated chains A (**A**), B (**B**), C (**C**),

and D (**D**). Mn^{II} and Fe^{II} ions are shown as purple and green spheres. Coordinated water molecules are shown as red spheres and labeled w1 and w2 in each view. Selected protein residues are shown in stick format. A $2F_o$-F_c map is shown in gray mesh (contoured at 1.2σ), and an F_o-F_c difference map is shown in red and green mesh (contoured at 3.0σ).

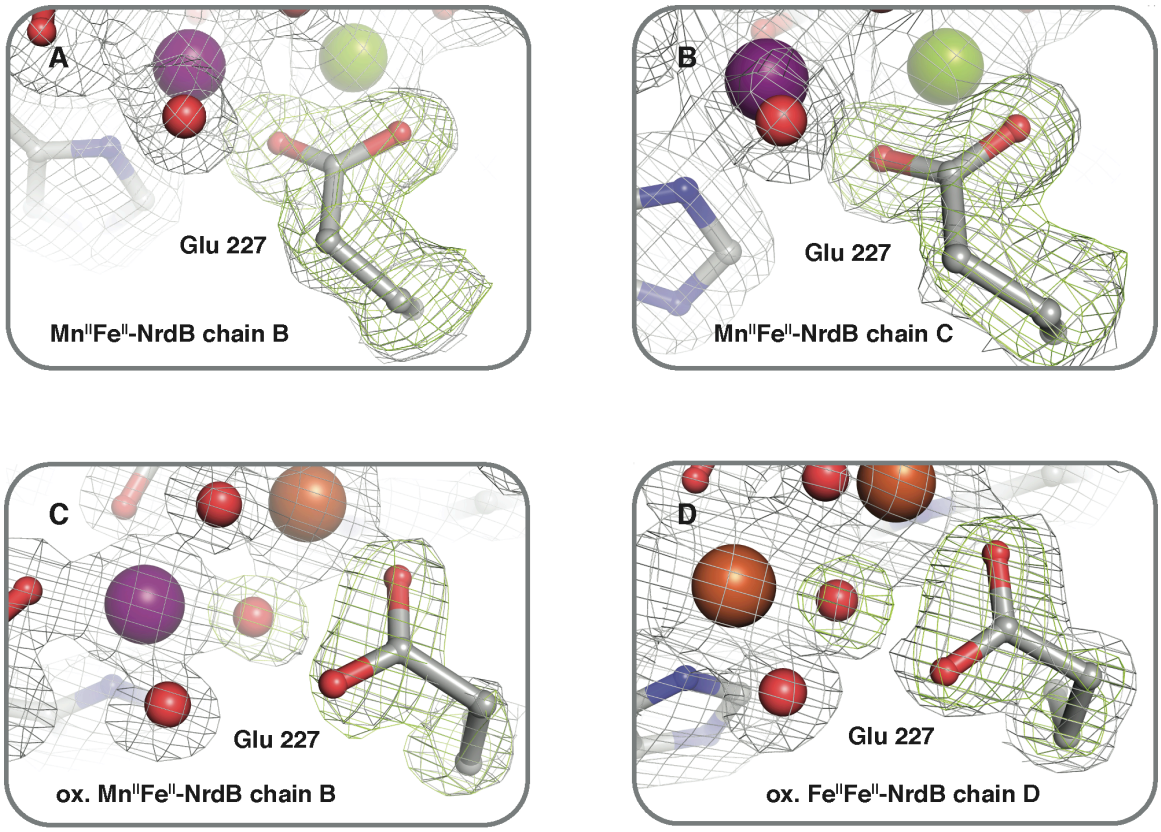

Figure S6. Zoomed-in views of the electron density map associated with bridging ligand Glu 227 in *Ct* Mn^{II}/Fe^{II}-β_2 (NrdB) and its oxidized form. To determine whether the difference density associated with Glu 227 in the $Mn^{II}Fe^{II}$-β_2 (NrdB) structure (**Figure S5**) might warrant modeling the residue in an alternate conformation, omit maps were generated for the side chain, as shown in (**A**) and (**B**) (green mesh, contoured at 5.5σ). These maps are consistent with the current model showing the residue coordinating both metal sites in a μ-η^1,η^2 interaction. To facilitate comparison, parts (**C**) and (**D**) show a similar omit map (green mesh, 4σ for (**C**) and 6.6σ for (**D**)) for the residue in datasets from oxidized protein samples (**Tables S7** and **S8**), in which the side chain binds the site 2 metal in monodentate fashion.

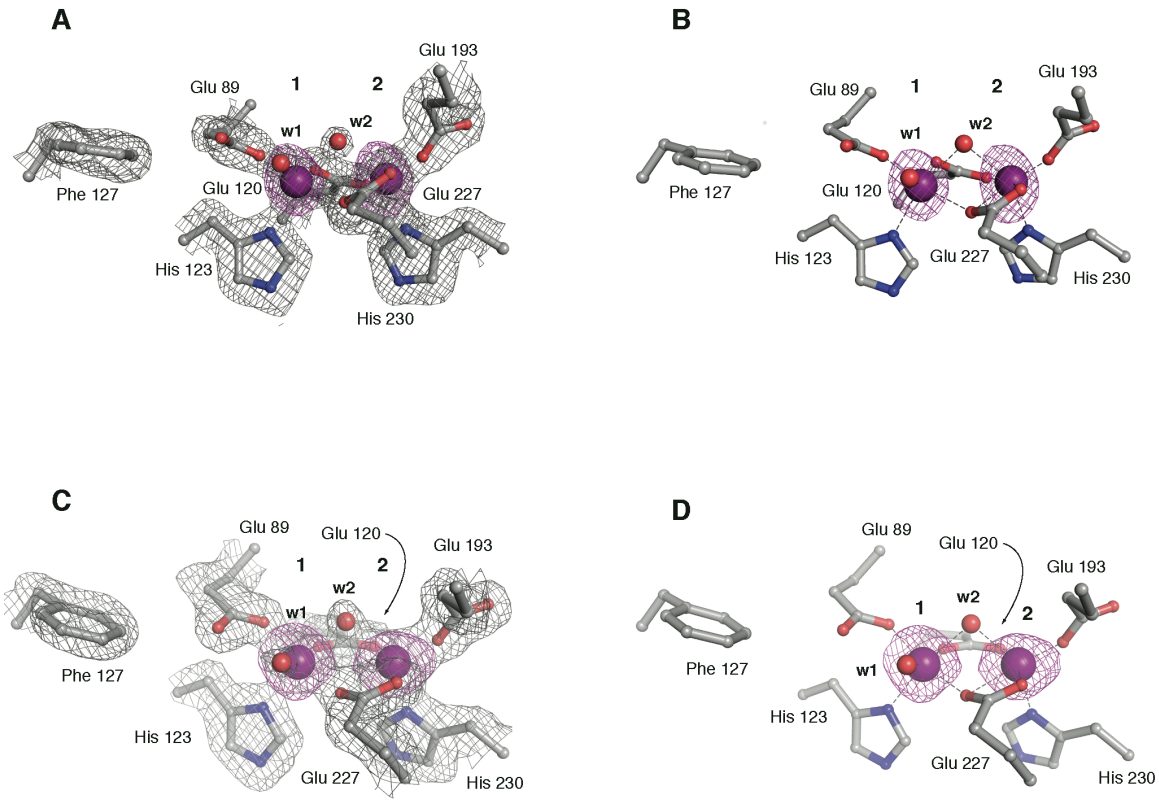

Figure S7. Electron density maps for a representative metal binding site of *Ct* β_2 crystallized with Mn^{II} alone at 1 equiv per β monomer (**Table S3**) in (**A**) and (**B**) and at 2 equiv per β monomer with an additional soak in 10 mM $MnCl_2$ after crystallization (**Table S4**) in (**C**) and (**D**). A $2F_o$-F_c map (contoured at 1.2σ) is shown in gray mesh and an Mn anomalous difference map (contoured at 4σ) is shown in purple mesh. Metal ion occupancies range from 40-70% in the 1 equiv Mn^{II} structure (**A**, **B**) and 70-90% in the structure with excess Mn^{II} (**C**, **D**).

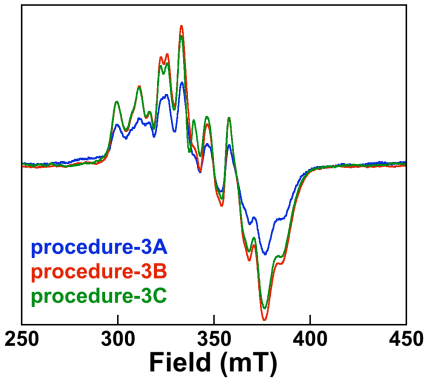

Figure S8. X-band EPR spectra of the dithionite-reduced, Mn^{III}/Fe^{III} forms of the protein used for the oxidized structure reported in **Figure 3B** of the main manuscript. A description of the sample preparation is provided in **Experimental Procedures**. The quantities of metals retained in each sample and the demonstrated activities are reported in **Table 2**. Spectrometer conditions were: 9.48 GHz microwave frequency, 100 KHz modulation frequency, 20 mW microwave power, 0.1 mT modulation amplitude, 14 ± 0.2 K temperature, 0.163 time constant, 167 s scan time.

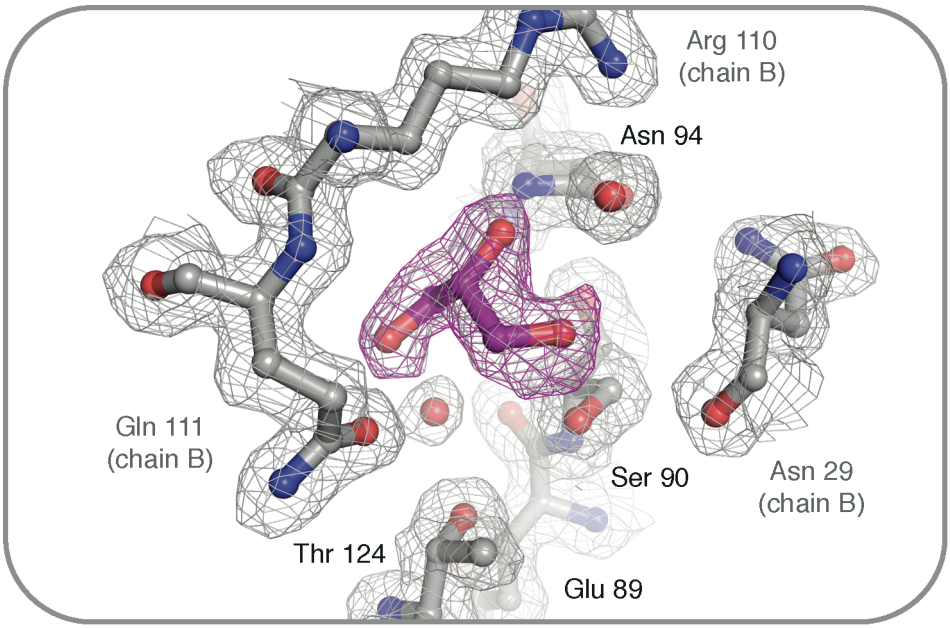

Figure S9. Electron density for a glycerol molecule bound in an interior pocket near the active site described in **Figure S4**. A $2F_o$-F_c map (contoured at 1.2σ) is shown in gray mesh, and an omit map (contoured at 4.6σ) is shown in purple mesh, both calculated from the dataset described in **Table S7**. This pocket is lined by hydrophilic side chains (Thr 124 and Ser 90) adjacent in the sequence to protein ligands to site 1 (Glu 89, His 123). Additionally, the glycerol molecule interacts with an Asn pair (Asn 94, Asn 29 from chain B) and other polar residues contributed by the adjacent chain. The glycerol molecule is derived from the protein storage buffer or cryoprotectant solution, but its binding site may be important as a metal ion or proton influx/efflux route.

SUPPORTING REFERENCES

1. Krissinel, E., and Henrick, K. (2004) Secondary-structure matching (SSM), a new tool for fast protein structure alignment in three dimensions. *Acta Crystallogr. D60*, 2256-2268.

2. Åberg, A., Nordlund, P., and Eklund, H. (1993) Unusual clustering of carboxyl side chains in the core of iron-free ribonucleotide reductase. *Nature 361*, 276-278.